

# Design-Induced Cyclic Effects in Event-related fMRI Experiments

Darcie A. P. Delzell<sup>a</sup>, Qihua Lin<sup>b</sup>, Richard F. Gunst<sup>\*c</sup>, William R. Schucany<sup>c</sup>, Wayne A. Woodward<sup>c</sup>,  
Patrick S. Carmack<sup>d</sup>, Jeffrey S. Spence<sup>b</sup>, and Robert W. Haley<sup>e</sup>

March 9, 2010

<sup>a</sup> *Department of Mathematics, Wheaton College, Chicago, IL, USA*

<sup>b</sup> *Department of Clinical Science, Biostatistics Division, University of Texas Southwestern Medical Center at Dallas, 5323 Harry Hines Boulevard, Dallas, TX 75390-8830, USA*

<sup>c</sup> *Department of Statistical Science, Southern Methodist University, P.O. Box 750332, Dallas, TX 75275-0332, USA*

<sup>d</sup> *Department of Mathematics, University of Central Arkansas, 201 Donaghey Avenue, Conway, AR 72035-5001, USA*

<sup>e</sup> *Department of Internal Medicine, Epidemiology Division, University of Texas Southwestern Medical Center at Dallas, 5323 Harry Hines Boulevard, Dallas, TX 75390-8874, USA*

\* Corresponding author. Department of Statistical Science, Southern Methodist University, P.O. Box 750332, Dallas, TX 75275-0332. Fax +1-214-768-4035  
*E-mail:rgunst@smu.edu (R. F. Gunst).*

## Abstract

In analyses of event-related functional magnetic resonance imaging (fMRI) experiments, detecting and adjusting for physiological, scanner, and unknown but repeatable noise components generally increase the power to detect the true fMRI signal. In a series of single-trial-type fMRI experiments, however, attempts to model unexpected cyclic trends were found to be unrelated to known physiological and scanner cycles and not due to the expected hemodynamic response. These unexpected cyclic trends were also found to be observable in more complex designs. Spectral and cepstral analyses attributed the cyclic trends to ripple effects induced by the choice of interstimulus intervals (ISIs) in the design. Further investigation exploring the effects of varying and randomizing the ISIs with and without noise found that, although the spectral and cepstral properties varied with the design, the frequency [periodicity] of the ripples remained relatively constant as a function of the ISIs. Cepstral analysis of an fMRI experiment, preferably in the design stage, can identify likely ripple effects that are not necessarily eliminated by randomizing the ISIs, thereby preventing possible loss of detection power due to inappropriately controlling for these surrogates of ISI design effects. Alternative designs can also be considered.

**Key Words:** Autocorrelated errors, cepstrum, cyclic trends, interstimulus intervals, ripple effect, spectrum

## 1 Introduction

Statistical features of the design of fMRI experiments must be tailored to the goals of the experiment. The type of stimuli, the expected evoked responses, measurement issues, and the selection of stimulus times (STs) or interstimulus intervals (ISIs, the time from the initiation of one stimulus to the initiation of the next one) must be carefully considered in order to maximize hemodynamic response detection power or estimation efficiency. This article investigates the effects of the choice of ISIs in an event-related fMRI experiment when the goals of an fMRI experiment include the fitting of a nonlinear hemodynamic response function (HRF).

Event-related fMRI experiments are generally considered preferable to experiments with block designs when concerns over possible habituation or anticipation could seriously violate the assumption of linear-time-invariant (LTI) hemodynamic responses (Dale and Buckner 1997). Liu et al. (2001) demonstrated that block designs are advantageous for signal detection in single-trial-type fMRI experiments, while event-related designs are preferable for estimating the HRF. These findings were supported for multiple-trial-type designs in Liu and Frank (2004) and in Liu (2004).

With respect to the selection of ISIs, Josephs et al. (1997) used relatively long (with respect to the volume acquisition time, TR), equally spaced ISIs in order to allow multiple acquisitions of the complete time course of each hemodynamic response. They alternated the onset times of the stimuli so that they were either between volume acquisitions or at the midpoint of the volume acquisitions. This was done so that the peaks and troughs of the HRF could be more accurately estimated. Price et al. (1999), using a fixed ISI and TRs between 1 and 2 times the ISI, demonstrated the importance of varying the onset times of the stimuli relative to the TR. They showed clear disadvantages of having the TR be an integer multiple of the ISI, leading to acquisition times that are the same relative times during the time course of the HRF. Serious underestimation or overestimation of the HRF can occur, along with the attendant loss of statistical power in tests for activation.

For designs with a constant ISI, Bandettini and Cox (2000) found that for event-related fMRI experiments that have stimulus durations shorter than 2 seconds the optimal ISIs ranged from 10 to 12 seconds. They observed that shorter ISIs caused the HRFs to overlap, resulting in a loss of signal amplitude relative to baseline and the presence of a “pseudo pre-undershoot” due to the failure of the HRF to return to baseline prior to the next stimulus. Birn et al. (2002) found that shorter ISIs, on the order of 2 seconds, were optimal for designs that permitted variable ISIs. This was also the conclusion of Dale (1999), who found that alternating between task and rest states as quickly as possible gave the best HRF estimation. There remain widely varying opinions regarding the choice of optimal statistical designs for fMRI experiments, and Dale’s (1999) comment remains valid: “It has been widely argued, based on empirical as well as theoretical evidence, that using ISIs of at least 15 sec is optimal and that using shorter ISIs results in a severe reduction in statistical power. However, numerous studies have shown highly reliable event-related fMRI response estimates using ISIs as short as seconds or less”.

The present article was motivated by the desire to select ISIs for a series of fMRI experiments on 1991 Persian Gulf War veterans. This extensive series of experiments is designed to better identify and define suspected brain abnormalities among veterans suffering from what is now termed the Gulf War Syndrome; see Haley et al. (2008) and the references therein. Of particular importance in some of these experiments is the desire to fit a statistical model that describes the form of the HRF. The model might use a canonical form for the HRF and fit only scale parameters or it might be a nonlinear form such as a two-gamma model in which location, scale, and shape parameters are to be estimated. In part, interest in fitting such nonlinear models results from the potential to detect differences in parametric maps of the parameter estimates, maps that might provide important characterizations of differences in the HRFs between syndrome and control groups.

During a pilot study of the test protocols on a single subject, a perplexing issue arose while fitting models to the fMRI data. This issue was confirmed with the testing of a second subject months later using the same protocol. The experiment consisted of having the subjects silently repeat nonsense words after hearing them. Figure 1 shows the fMRI time courses from 4 voxels in the auditory cortex from the second subject. The time courses are of residuals from a quadratic drift fit to the fMRI signals, with a separate fit for each voxel. Superimposed is a nonparametric second-order loess curve fit (Cleveland and Devlin 1988, R Development Core Team 2008; span = 0.25) to the residuals, with a separate fit to each time course. The unexpected issue is the apparent cyclic behavior in the time courses. Cyclic behavior like this not only appeared in a large number of voxels in the auditory cortex but also in the average across 161 voxels chosen from a preliminary assessment of the presence of an HRF signal. Moreover, the cyclic pattern remained even after the fitting of a six-parameter two-gamma HRF to the drift residuals. The similarity of this cyclic behavior in many of the individual voxels, in the averages, and in the residuals for both of the subjects was unexpected.

*[Insert Figure 1]*

Many articles on model fitting for fMRI data indicate the presence of low-frequency behavior of the observed signal, often ascribed to scanner instabilities, patient cardiac and respiratory cycles, or

to unknown temporal confounds (e.g., Friston et al. 1995, Holmes et al. 1997, Zarahn et al. 1997, Friston et al. 2000, Liu et al. 2001, Lundquist 2008). Suggestive, but certainly not conclusive, in the low-frequency trend in the cyclic patterns in Fig. 1 is that the patterns might be due to the statistical design itself; i.e., to the choice of ISIs. At the bottom of each graph in Fig. 1, the triangles indicate the stimulus times. There are clusters of relatively rapid stimulus times and gaps of less frequent stimulus times. The reason the cyclic patterns, and the possibility of the design causing them, are so surprising is that the ISIs were randomly and relatively uniformly selected from candidate ISIs of 2,4,...,20 seconds.

Properly accounting for trends in the statistical modeling of fMRI data is required for the computation of correct standard errors and, hence, the validity of statistical inferences. Little is known about the effects of the choice of ISIs on the possible inducement of cyclic trends. The intent of this article is to investigate the effects of such trends and their accommodation in the modeling of fMRI data.

## 2 Methods

Cyclic behavior in fMRI time series can be induced in a number of ways. The possible effects of equipment and patient physiology have been well documented (see the references cited above). While ascribing such cyclic behavior to causes is often less important than properly accommodating it in the statistical analysis of the resulting data, identifying one important cause can sometimes alleviate the problem altogether – when the cause is the design of the experiment through the selection of ISIs.

Bogert et al. (1962) define *echos* as time series that are composed of delayed and possibly amplified versions of a fundamental component series. Similarly, Shumway et al. (1998) define *ripple events* as signals “that are often regularly grouped in space and time” . In both contexts, signals are produced in a regular, repeated fashion that affect the spectral properties of observed time series. Of importance to the consideration of modeling fMRI time series is that the ripple effects can induce periodic behavior of the observed time series. With fMRI time series, the ripple

effects are produced by repeated stimuli causing repeated activation of brain regions.

For a stimulus-induced ripple event with  $m$  delays  $T_j$ , the resulting time series observed at times  $t_i$  can be expressed as

$$z(t_i) = \sum_{j=0}^m y(t_i - T_j) + e_i, \quad (1)$$

where  $T_0 = 0$  and  $y(t) = 0$  if  $t < 0$ . If the sampling times are assumed to be equally spaced with sampling interval  $\Delta$ , then  $t_i = i\Delta$ . The HRF ripples can be modeled as

$$y(t_i - T_j) = h(t_i - T_j; \boldsymbol{\theta}) + v_{ij}, \quad (2)$$

where  $h(t; \boldsymbol{\theta})$  is the HRF. The errors  $e_i$  and  $v_{ij}$  will be specified subsequently. The functional form of the two-gamma HRF used in this work is

$$h(t; \boldsymbol{\theta}) = c_1 ([w_1(t) \exp\{1 - w_1(t)\}]^{a_1} - c_2 [w_2(t) \exp\{1 - w_2(t)\}]^{a_2}), \quad (3)$$

where  $w_k(t) = t/d_k$  for  $k = 1, 2$ ;  $h(t; \boldsymbol{\theta}) = 0$  for  $t < 0$ ; and  $\boldsymbol{\theta} = (a_1, a_2, c_1, c_2, d_1, d_2)$ . If all the parameters except  $c_1$  are specified, (3) is referred to as a canonical HRF. Calculations reported below using (3) have parameter values  $\boldsymbol{\theta} = (12.98, 27.01, 5.87, 13.55, 5.08, 0.47)$ , values obtained from the pilot study.

The *cepstrum* was introduced by Bogert et al. (1962) to detect echo or ripple effects. They recommended treating the log-spectrum of the data as one would a time series, but with frequency replacing time. Let  $\log P_z(f)$  denote the log-spectrum. As a function of the frequency  $f$ , the log-spectrum is approximately

$$\log P_z(f) \approx \log P_y(f) + \log \left[ \sum_{j=1}^m \sum_{k=1}^m \cos \{2\pi f (T_j - T_k)\} \right]. \quad (4)$$

If the ripple delays are equally spaced, then  $T_{j+1} - T_j = \tau$  and

$$\log P_z(f) \approx \log P_y(f) + \log\{(m+1) + 2 \sum_{j=1}^m (m+1-j) \cos(2\pi f j \tau)\}, \quad (5)$$

which has multiple cyclic patterns with periods of  $1/j\tau$ ,  $j = 1, 2, \dots, m$ . Hence, the cepstrum, which is the spectrum of  $\log P_z(f)$ , has, apart from noise effects, peaks at the delays  $T_j - T_k$ . For constant delay ripples, the peaks occur at multiples of the constant delay  $\tau$  with decreasing magnitudes. The clarity with which the cepstrum enables the identification of ripples depends on the relative magnitudes of the first and second terms in (4) and (5), as well as the magnitudes of the error terms in (1) and (2).

### 3 Results

#### 3.1 Noise-free Signals

Ripple effects are most strikingly evident when ISIs are equally spaced and the model contains no random errors. Figure 2 shows the time course, spectrum, and two cepstral plots for a signal consisting of the two-gamma HRF (3) convolved with stimuli equally spaced every 30 sec. The time course is  $T = 300$  sec. with sampling every 1 sec. for this time course and all others except those using the stimulus vector from the pilot study, for which  $T = 304$  sec. and samples are taken every 2 sec. Figure 2(a) shows the time course, with the stimulus times shown at the bottom of the graph. The spectrum (calculated using the function *spectrum* in R: R Development Core Team 2008) in Fig. 2(b) highlights the cyclic pattern in the ripples, with the decreasing peaks occurring at frequencies that are multiples of  $1/\tau = 1/30 = 0.033$ . Figure 2(c) shows the graph of the cepstrum calculated from the detrended log-spectrum, where the detrending was accomplished using a nonparametric loess fit with a span of 0.25. The cepstral values are graphed as a function of ripple delay times. The dominant peak is at 30 sec. and smaller peaks occur at multiples of this primary ripple delay time. Peaks occurring at ripple delay times are often more readily apparent

when the cepstrum is calculated from the original spectrum, not the log-spectrum. Figure 2(d) illustrates the enhanced clarity of the peaks when the cepstrum is calculated from the spectrum. This enhanced clarity is especially important when the signals are noisy.

*[Insert Figure 2]*

In order to minimize anticipation or habituation, varying the ISIs in an fMRI design is widely advocated. Figure 3 shows plots of the spectrum and cepstrum for a design with three ISIs: 4, 5, and 8 sec. In Figs. 3(a) and (b) the design consists of cyclic repetitions of the ISIs: 4, 5, 8, 4, 5, 8, etc. Note that a complete cycle of all 3 ripple delays occurs every 17 sec. The individual delay times of 4, 5, and 8 sec. are not identifiable in either figure. Rather, the complete-cycle peaks are evident in the spectrum in Fig. 3(a) with decreasing magnitudes at frequencies that are close to multiples of the primary frequency  $f = 1/17$ . The complete-cycle ripple effects are evident in the cepstral plot in Fig. 3(b), where the primary peak is again close to 17 sec. The delay time of 17 sec. is indicated by the blue line and the secondary peaks at multiples of 17 sec. are indicated by the red lines. Less smoothing of the cepstrum (a modified Daniell smoothing kernel with parameters (1,1) in R was used) would make these peaks even more pronounced. Some of the spectral and cepstral peaks do not occur exactly at frequencies that are multiples of  $1/17$  and delay times that are exact multiples of 17 sec., respectively, due to the equally spaced mapping of the frequencies to and from the frequency domain interval of  $[0, 0.5]$ . Nevertheless, the dominant complete-cycle ripple delays at or near 17 sec. are clearly evident.

*[Insert Figure 3]*

Figures 3(c) and (d) show the spectrum and the cepstrum for a randomization of the design with ISIs of 4, 5, and 8 sec. The randomization was performed separately within each 17 sec. complete cycle in order to ensure that each of the ISIs occur approximately an equal number of times while retaining the complete-cycle delay time of 17 sec. The 17 sec. complete-cycle peak is evident in the spectrum in Fig. 3(c) but the subsequent peaks at harmonics of  $f = 1/17$  are not clearly depicted. There is a dominant peak in the cepstrum in Fig 3(d) but it is not at a time delay of 17 sec. It

occurs at approximately 25 sec. The other, smaller peaks would not be sufficient to identify the complete-cycle ripple delay of 17 sec. or any of the individual ripple delays. Figures 3(c) and (d) depict only one possible realization of the effects of randomization. Other randomizations produce peaks at different delay times.

Figure 4 illustrates a final variation on the spectrum and cepstrum for cyclic versions of the ISIs. The signal was generated by repeating an ISI sequence of  $\{10, 20, 20, 10\}$ . Superimposed in red on the signal in Fig. 4(a) is a loess fit similar to that in Fig. 1. Superimposed in blue is a sine function with period of 60 sec., the combined period of the ISIs. The two curves overlap except at the very extreme ends of the graph. One might expect from Fig. 4(a) and the results shown in Figs. 3(a) and (b) that the spectrum and the cepstrum would have peaks at  $1/\tau = 1/60 = 0.017$  and  $\tau = 60$  sec.), respectively. However, the primary peaks in the spectrum highlight the individual ripple delays, 10 and 20 sec. The peak with the greatest magnitude is at a frequency of  $1/20$ . The peak with the other dominant magnitude is at  $f = 1/10$ , which is a harmonic ( $f = 2/20$ ) of the 20 sec. delay time frequency. Barely noticeable are small peaks at additional harmonics  $f = 3/20$  and  $4/20$ . The cepstrum has 3 primary peaks, at 20, 40, and 60 sec., and a smaller one at 80 sec. These are all multiples of the primary delay time, 20 sec.

*[Insert Figure 4]*

The spectrum in Fig. 5(a) for the noise-free signal using the stimulus times from the pilot study mentioned in the introduction does not indicate a frequency that is identifiable with ripple delays. Figure 5(a) has the appearance of a spread spectrum over peak signal frequencies that range approximately from 0.05 to 0.08 Hz. That there is a range of frequencies is not unexpected because there are 10 different ISIs in the stimulus vector. The dominant peak in the cepstrum in Fig. 5(b) at approximately 40 sec. is longer than the individual delay times suggested by peaks in the spectrum, 10 - 20 sec. The primary peak in the cepstrum is due to the apparent cycle in the spread spectrum that is highlighted by the red loess fit in Fig. 5(a). The spread spectrum encompasses a range of approximately 0.13 Hz, which corresponds to a period in the original time scale of 39 sec. Although the nonparametric loess fits in Fig. 1 are not truly cyclical, the long delay

time indicated in Fig. 5(b) is consistent with the visually suggestive long periods in Fig. 1.

*[Insert Figure 5]*

### 3.2 Effects of Noise

There are two levels of noise specified in (1) and (2). Each can affect the ability to identify cyclic patterns in fMRI data due to the selection of ISIs. The noise in (1) can be depicted as measurement error; i.e., due to all sources that prevent the hemodynamic response  $y(t)$  from being observed exactly. These sources include patient movements, scanner imperfections, etc. The HRF noise in (2) includes patient physiology, magnetic field inhomogeneities, improper specification of the approximating HRF, etc. that prevent the HRF from each stimulus from being exactly the same in the absence of measurement error. While most statistical models include only the errors in (1), these two types of error have very different effects on the ability to identify cyclic patterns in fMRI data that are due to the design.

To illustrate the effects of these two types of noise, the ISIs of Figs. 2 and 4 were used with the same HRF but with noise added. In Fig. 6(a) and (b) the spectrum and cepstrum are shown when only measurement error with  $\sigma = 3$  from (1) is added. The ripple effects that are clearly evident in the spectrum in Fig 2(b) are masked in Fig 6(a) due to the presence of measurement errors. The cepstrum in Fig 6(b) more clearly indicates the presence of ripple delays of around 30 sec. in spite of the presence of measurement errors.

*[Insert Figure 6]*

When HRF noise from (2) with  $\sigma = 2$  is also added, the combined sources of noise further mask the clarity with which the ripples are depicted in the spectrum in Fig. 6(c). The cepstrum in Fig 6(d), however, again clearly identifies the single ripple delay time of 30 sec.

The clarity with which the ISI cyclic behavior is observable in the spectrum also changes with

multiple ISIs when the signal is itself noisy. Figures 7(a) and (b) display the spectrum and cepstrum for signals produced from the cyclically repeated ISI sequence 10, 20, 20, and 10 sec. when only measurement error is added. The dominant peaks in Figs. 4(b) and (c) are still evident in Figs. 7(a) and (b); however, when both HRF noise and measurement error are modeled, the spectrum in Fig 7(c) does not indicate any ripple effects. The cepstrum in Fig 7(d) does highlight the ripple delay time of 20 sec., along with additional peaks at multiples of 20 sec.

*[Insert Figure 7]*

The spectra for the signal with random errors using the stimulus times from the pilot study are very different and depend on whether only measurement errors are added, Fig. 8(a), or both HRF errors and measurement errors are added, Fig. 8(c). These graphs can look very different with each realization of the errors. While the cepstral plots in Figs. 8(b) and (c) have noticeable differences, there are some features of each that enable ripple effects that have delay times close to those in the error-free signal to be identified. In Fig. 5(b) a dominant peak at 40 sec. and a smaller one at 60 sec. were clearly visible. In Fig. 8(b) the dominant peak occurs at near 40 sec. The secondary peak at 60 sec. cannot be determined from this cepstrum. The peaks in Fig. 8(d) are at delay times near 40 and 60 sec. but the relative magnitudes of the peaks are different from those in Fig. 5(c).

*[Insert Figure 8]*

An interesting feature of Figs. 6 - 8 is the effect of noise on the presence and detection of ripple effects. In each of the figures, the addition of noise increases the magnitudes of the spectral and cepstral peaks. This is evident from the scales on the vertical axes. Measurement error alone produces spectral and cepstral plots that have peak magnitudes similar to or greater than the magnitudes in the corresponding plots in Figs. 2, 4, and 5. Addition of HRF noise to the measurement errors greatly increases the magnitudes of the peaks.

### 3.3 Diagnosing Ripple Effects

Pivotal to the determination of whether an observed cyclic pattern in fMRI data is due to the design through the ISIs or due to scanner or patient cycles are the ISIs themselves. A cepstrum can be calculated for the vector of stimulus times and compared to the cepstrum from the observed fMRI data. Figure 9 displays cepstra for the stimulus times in all of the examples covered: (a) 30 sec. ripple delays; (b) cyclically permuted ripple delays of 4, 5, and 8 sec.; (c) cyclically permuted ripple delays of 10, 20, 20, and 10 sec.; and (d) the random uniform ISIs of the pilot study.

The major peaks in Figs. 9(a) - (c) are all consistent with the corresponding cepstral peaks in the error-free signals and the signals containing errors. In a few instances the relative magnitudes of the peaks change but the ripple delay times are readily identified. In Fig. 9(d) the primary peak at the delay time of 40 sec. is prominent. A secondary one at approximately 60 sec. is also visible.

*[Insert Figure 9]*

Figure 10 displays cepstra that were calculated from the 4 individual voxels in Fig. 1. All of these cepstra have primary peaks near 40 sec. and smaller but visible ones between 60 and 70 sec. These ripple delay times are consistent with those of the stimulus times and the calculations in Figs. 5 and 8.

*[Insert Figure 10]*

## 4 Discussion

The key to correctly detecting that cyclic patterns in fMRI data are due to the design and not due to scanner or subject cycles is understanding that the design and its properties are known. To the extent that the observed fMRI data exhibit cyclic patterns similar to those in the stimulus times, the observed patterns are a natural result of the design and are not features that need to be

modeled or accommodated. Modeling natural cyclic patterns that are due solely to the selection of ISIs could reduce the ability to correctly model nonlinear HRFs because some of the actual signal might be confounded with the cyclic pattern of the ISIs. Genuine sinusoidal patterns due to patient effects, scanner effects, or the measurement process should be modeled because they contribute to external noise from known sources that could mask the HRF signal.

It might be expected that randomization of the ISIs would compensate for any deleterious effects of the ISIs on the detection of the fMRI signal. While this might be true, whether this is true depends on the randomization pattern of the ISIs. The properties of the stimulus pattern, through the use of spectral and cepstral analysis, should be performed in order to assess the effects of the ISIs, preferably prior to the final selection of a design.

The two sources of error, measurement error and HRF noise, were introduced in order to investigate the extent to which different sources of error affect cepstral plots and the identification of ripple delay times. Comparisons of the results in Figs. 6 - 8 indicate that the cepstra do indeed change but the identification of the ripple delay times is remarkably stable. This is especially true for the primary ripple delay times in Figs. 6 and 7 for which there are repeatable complete-cycle ripple times. The addition of measurement error and HRF noise generally enhances the ripple effects.

The figures in this article demonstrate that the spectra and the cepstra highlight different cyclic properties of a time series, especially in the presence of substantive noise. The importance of a cepstral analysis is that it can help ascertain whether the choice of ISIs causes a ripple effect in fMRI data. If cyclic behavior is detected for a design and such behavior can be related to the ISI pattern, there is no need to model the cyclic trend and adjust the model for the fitted pattern. If a cepstral analysis of stimulus times for a proposed design indicates the likelihood of cyclic behavior in the resulting fMRI data, alternative designs can be investigated prior to selecting a final design.

## Acknowledgments

This study was supported by VA IDIQ contract number VA549-P-0027 awarded and administered by the Dallas, TX VA Medical Center. The content of this paper does not necessarily reflect the position or the policy of the U.S. government, and no official endorsement should be inferred. The authors would also like to thank Dr. Sergey Cheshkov for insightful comments on this work and Joel O’Hair and Ohn Jo Koh for their valuable computational assistance.

## References

- Atkinson, A.C., Donev, A.N., and Tobias, R.D. 2007. *Optimum Experimental Designs, with SAS*, Oxford Univ. Press, New York.
- Bandettini, P. A. and Cox, R. W. 2000. Event-Related fMRI Contrast When Using Constant Interstimulus Interval: Theory and Experiment, *Magnetic Resonance in Medicine* **43**: 540-548.
- Birn, R.M., Cox, R.W., and Bandettini, P.A. 2002. Detection versus Estimation in Event-related fMRI: Choosing the Optimal Stimulus Timing, *NeuroImage* **15**: 252-264.
- Bogert, B.P., Healey, M.J.R., and Tukey, J.W. 1962. The Quefrency Alanysis of Time Series for Echos: Cepstrum, Pseudo-Autocovariance, Cross-Cepstrum and Saphe Cracking, *Proceedings of a Symposium on Time Series Analysis*. ed. M. Rosenblatt, Wiley, New York, 209-243. Reprinted in Brillinger, D.R. (ed.) 1984. *The Collected Works of John W. Tukey, Volume I*, Wadsworth, Belmont, CA, 445-493.
- Buracas, G.T. and Boynton, G.M. 2002. Efficient Design of Event-Related fMRI Experiments Using M-Sequences, *NeuroImage* **16**: 801-813.
- Burock, M.A., Buckner, R.L., Woldorff, M.G., Rosen, B.R., and Dale, A.M. 1998. Randomized Event-related Experimental Designs Allow for Extremely Rapid Presentation Rates Using Finc-

- tional MRI, *NeuroReport* **9**: 3735-3739.
- Buxton, R.B., Liu, T.T., Martinez, A., Frank, L.R., Luh, W.-M., and Wong, E.C. 2000. Sorting Out Event-related Paradigms in fMRI: the Distinction Between Detecting and Activation and Estimating the Hemodynamic Response, *NeuroImage* **11**: S457.
- Cleveland, W.S. and Devlin, S.J. 1988. Locally Weighted Regression: An Approach to Regression Analysis by Local Fitting, *J. Amer. Stat. Assn.* **83**: 596-610.
- Dale, A.M. 1999. Optimal Experimental Design for Event-related fMRI, *Hum. Brain Map.* **8**: 109-114
- Dale, A.M. and Buckner, R.L. 1997. Selective Averaging of Rapidly Presented Individual Trials Using fMRI, *Hum. Brain Map.* **5**: 329-340.
- Friston, K.J., Holmes, A.P., Poline, J-B, Grasby, P.J., Williams, S.C.R., Frackowiak, R.S.J., and Turner, R. 1995. An Analysis of fMRI Time-Series Revisited, *NeuroImage* **2**: 45-63.
- Friston, K.J., Josephs, O., Zarahn, E., Holmes, A.P., Rouquette, S., and Poline, J.-B. 200. To Smooth or Not to Smooth, *NeuroImage* **12**: 196-208.
- Friston, K.J., Zarahn, Z., Josephs, O., Henson, R.N.A., and Dale, A.M. 1999. Stochastic Designs in Event-Related fMRI, *NeuroImage* **10**: 607-619.
- Glover, G.H. 1999. Deconvolution of Impulse Response in Event-Related BOLD fMRI, *NeuroImage* **9**: 416-429.
- Hagberg, G.E., Zito, G., Patria, F., and Sanes, J.N. 2001. Improved Detection of Event-Related Functional MRI Signals Using Probability Functions, *NeuroImage* **14**: 1193-1205.
- Haley, R.W., Spence, J.S., Carmack, P.S., Gunst, R.F., Schucany, W.R., Petty, F., Devous, M.D. Sr., Bonte, F.J., and Trivedi, M.H. 2008. Abnormal Response to Cholinergic Challenge in Chronic Encephalopathy from the 1991 Gulf War, *Psychiatry Research: Neuroimaging* **171**: 207-220.

- Holmes, A.P., Josephs, O., Buchel, C., and Friston, K.J. 1997. Statistical Modeling of Low-Frequency Confounds in fMRI, *NeuroImage* **5**: S480.
- Josephs, O., Turner, R., and Friston, K. 1997. Event-Related fMRI, *Hum. Brain Map.* **5**: 243-248.
- Liu, T.T. 2004. Efficiency, Power, and Entropy in Event-related fMRI with Multiple Trial Types, Part II: Design of Experiments, *NeuroImage* **21**: 401-413.
- Liu, T.T. and Frank, L.R. 2004. Efficiency, Power, and Entropy in Event-related fMRI with Multiple Trial Types, Part I: Theory, *NeuroImage* **21**: 387-400.
- Liu, T.T., Frank, L.R., Wong, E.C., and Buxton, R.B. 2001. Detection Power, Estimation Efficiency, and Predictability in Event-Related fMRI, *NeuroImage* **13**: 759-773.
- Lundquist, M.A. 2008. The Statistical Analysis of fMRI Data, *Statistical Science* **23**: 439-464.
- Price, C.J., Veltman, D.J., Ashburner, J., Josephs, O., and Friston, K.J. 1999. The Critical Relationship Between the Timing of Stimulus Presentation and Data Acquisition in Blocked Designs with fMRI, *NeuroImage* **10**: 36-44.
- R Development Core Team 2008. *R: A Language and Environment for Statistical Computing*. R Foundation for Statistical Computing, Vienna.
- Seber, G.A.F. and Wild, C.J. 1989. *Nonlinear Regression*. Wiley, New York.
- Shumway, R.H, Baumgardt, D.R., and Der, Z.A. 1998. A Cepstral F Statistic for Detecting Delay-Fired Seismic Signals. *Technometrics* **40**: 100-110.
- Wager, T.D. and Nichols, T.E. 2003. Optimization of Experimental Design in fMRI: A General Framework Using a Genetic Algorithm. *NeuroImage* **18**: 293-309.
- Zarahn, E., Aguirre, G.K., and DEsposito, M.D. 1997. Empirical Analyses of BOLD fMRI Statistics: I. Spatially Unsmoothed Data Collected under Null-Hypothesis Conditions. *NeuroImage* **5**: 179-197.

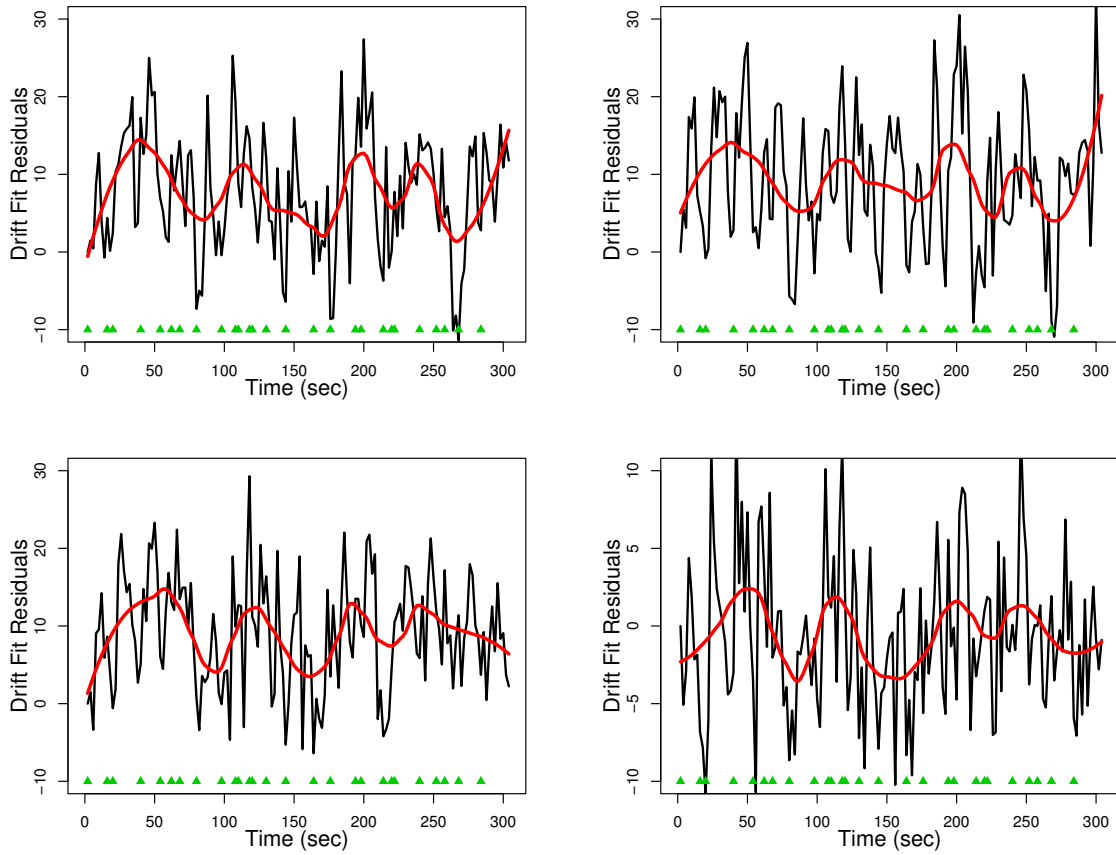


Fig. 1: Residuals from a quadratic drift fit for 4 voxels in the auditory cortex. Nonparametric loess curve fit in red. Stimulus activation times indicated by the green triangles.

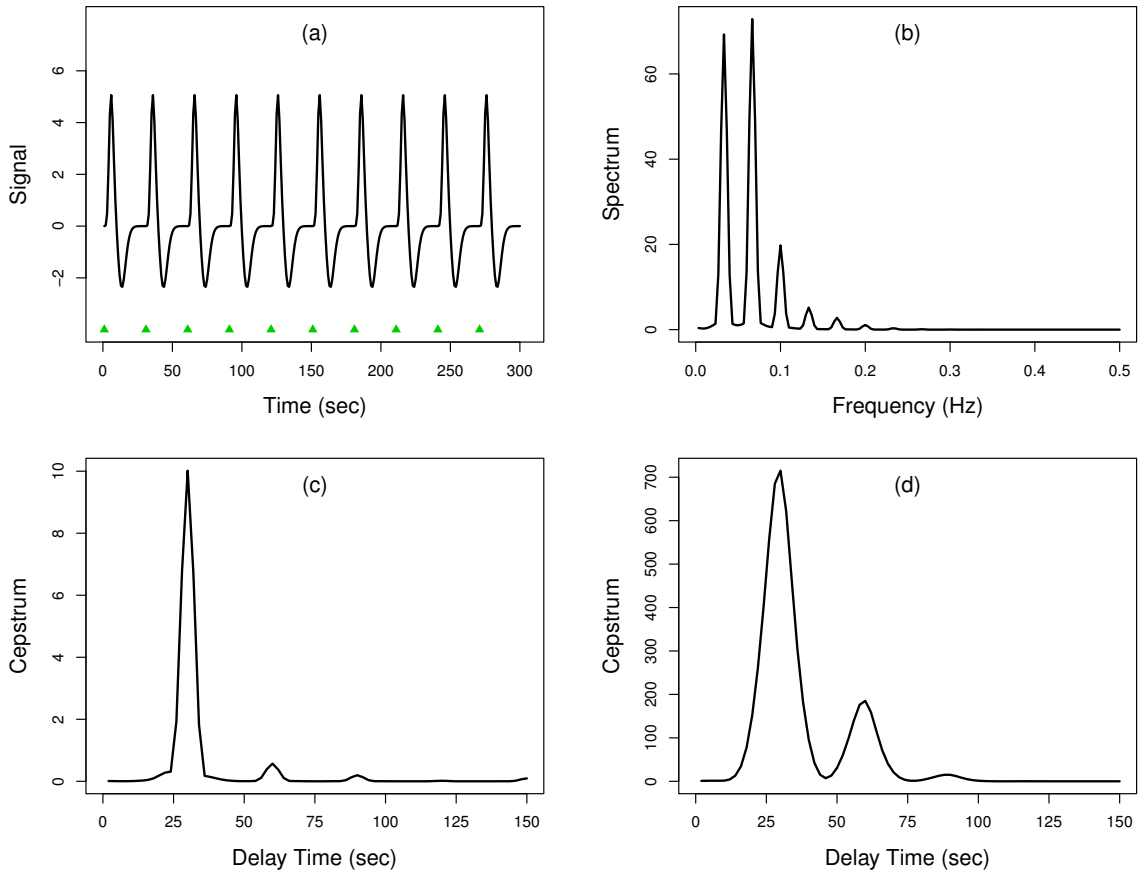


Fig. 2: Noise-free HRF signal with equally spaced ( $\tau = 30$  sec.) stimulus times. (a) Time course with stimulus activation times indicated by the green triangles; (b) Spectrum with peaks at multiples of  $1/\tau$ ; (c) Cepstrum (i.e., spectrum of the detrended log-spectrum) with decreasing peaks at multiples of the 30 sec. ripple delay time; (d) Cepstrum of the detrended spectrum (i.e., spectrum of the detrended spectrum).

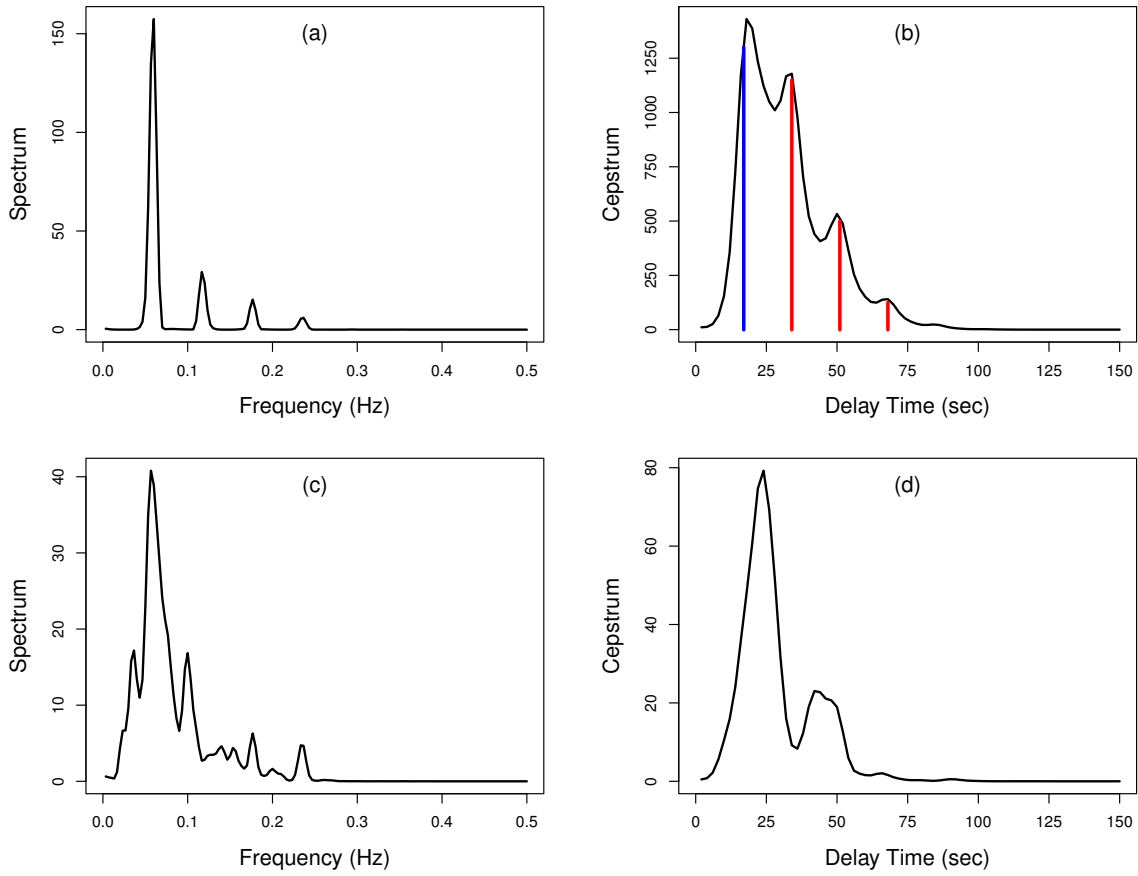


Fig. 3: Noise-free HRF signal with cyclically repeated ISIs of 4, 5, and 8 sec. (a) Spectrum with decreasing peaks at or near frequency multiples of  $f = 1/17$ ; (b) Cepstrum of the detrended spectrum with complete-cycle delay time of 17 sec. indicated by the blue line, multiples of the delay time by the red lines; (c) Spectrum for randomized ISIs; (d) Cepstrum of the detrended spectrum for randomized ISIs.

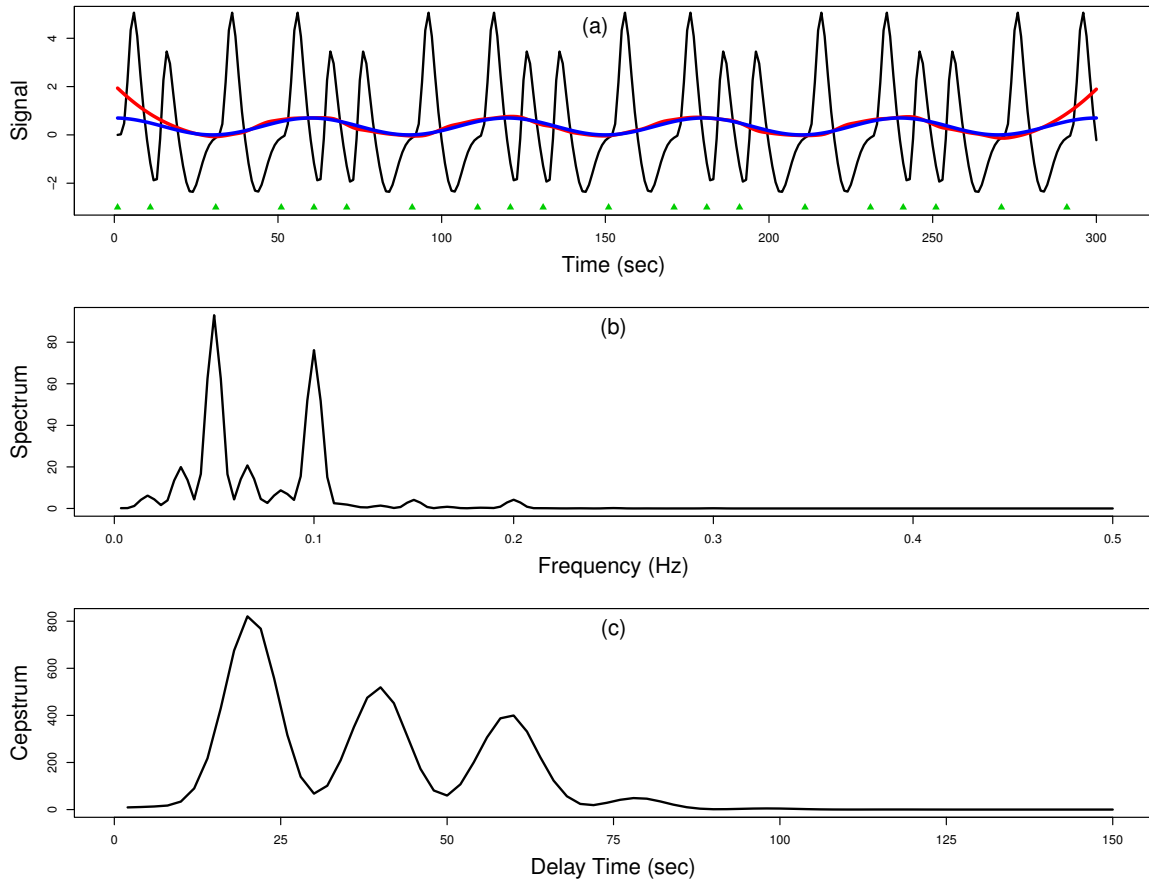


Fig. 4: Noise-free HRF signal with repeated ISI sequence of  $\{10, 20, 20, 10\}$ . (a) Time course with stimulus activation times indicated by the green triangles, loess fit indicated by the red curve, and approximating sine function indicated by the blue curve; (b) Spectrum with dominant peaks at  $f = 1/20$  and  $f = 1/10$ ; (c) Cepstrum of the detrended spectrum with peaks at multiples of 20 sec.

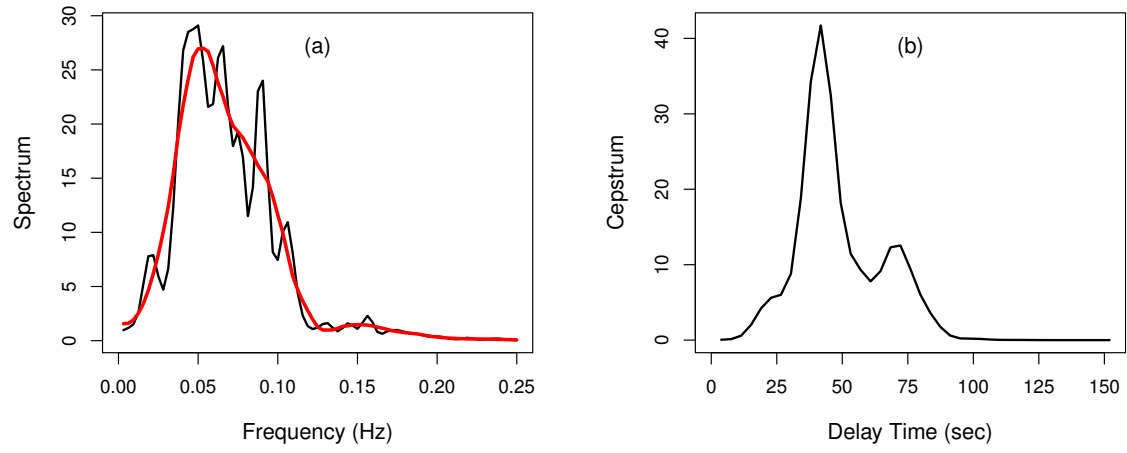


Fig. 5: Noise-free HRF signal using the pilot study stimulus times. (a) Spectrum with nonparametric loess fit in red; (b) Cepstrum of the detrended spectrum.

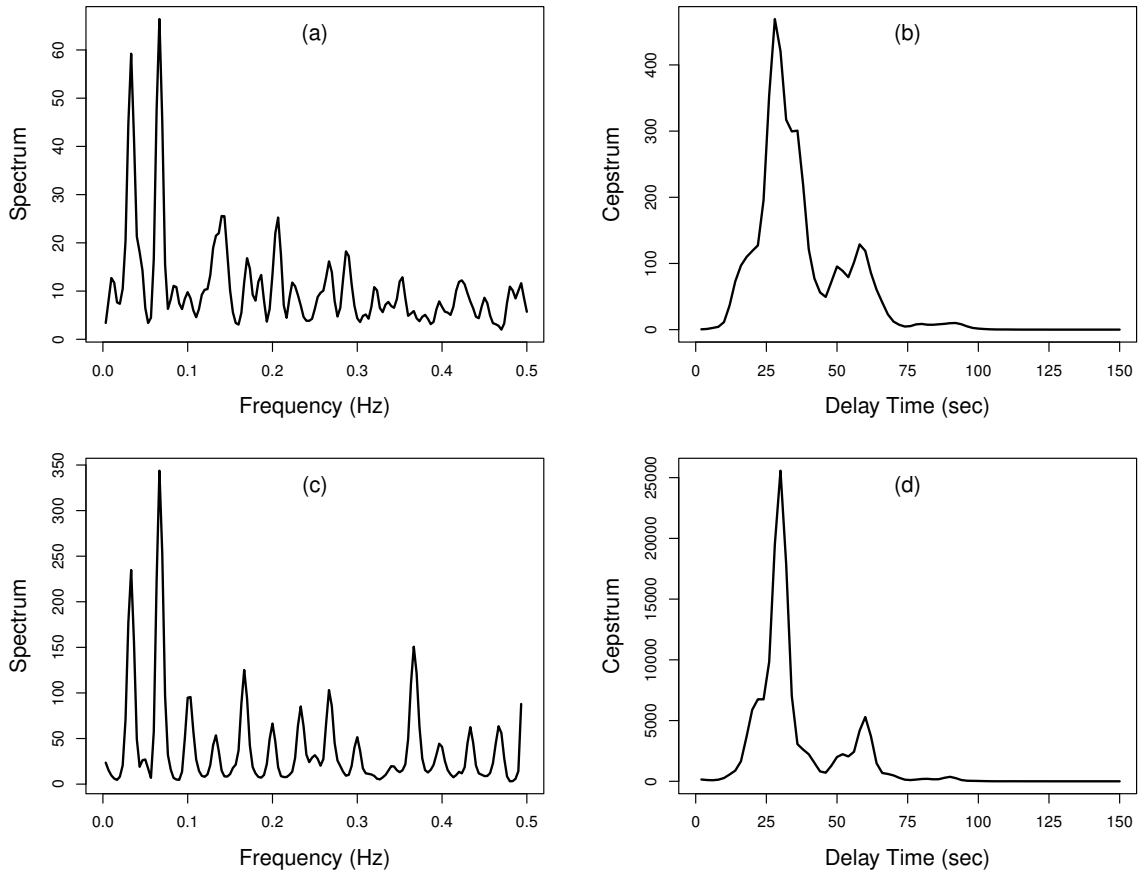


Fig. 6: HRF signal with equally spaced (30 sec.) stimulus times and noise. (a) Spectrum with only measurement error; (b) Cepstrum of the detrended spectrum, with only measurement error; (c) Spectrum with HRF noise and measurement error; (d) Cepstrum of the detrended spectrum, with HRF noise and measurement error.

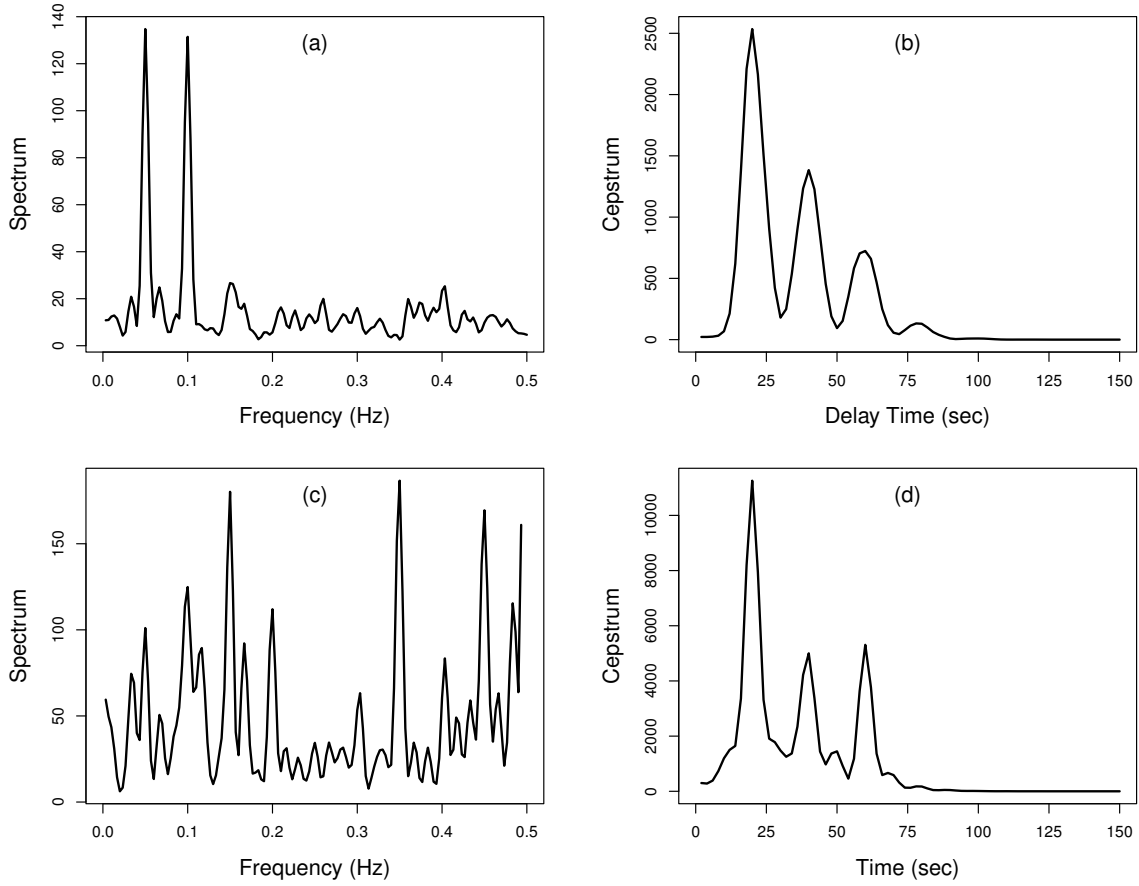


Fig. 7: HRF signal with repeated ISI sequence of  $\{10, 20, 20, 10\}$  and noise. (a) Spectrum with only measurement error; (b) Cepstrum of the detrended spectrum, with only measurement error; (c) Spectrum with HRF noise and measurement error; (d) Cepstrum of the detrended spectrum, with HRF noise and measurement error.

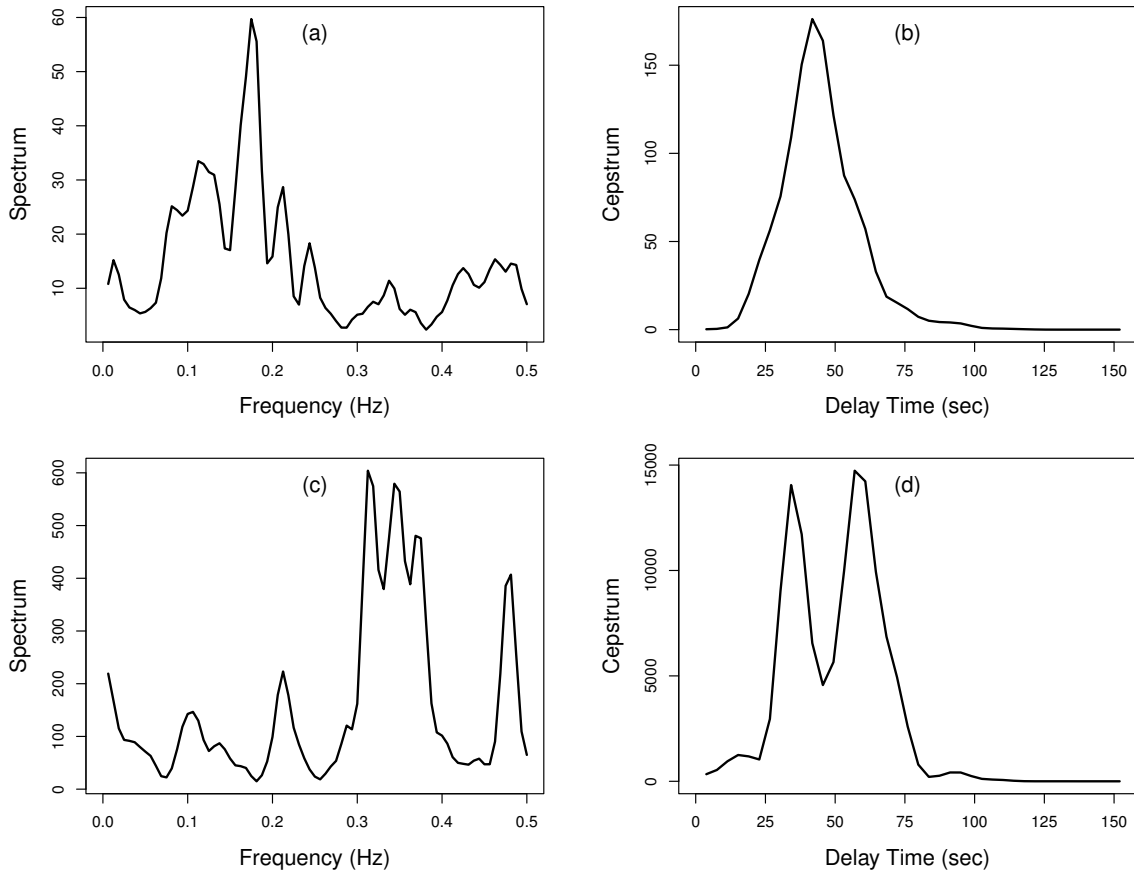


Fig. 8: HRF signal using the pilot study stimulus times and noise. (a) Spectrum with only measurement error; (b) Cepstrum of the detrended spectrum, with only measurement error; (c) Spectrum with HRF noise and measurement error; (d) Cepstrum of the detrended spectrum, with HRF noise and measurement error.

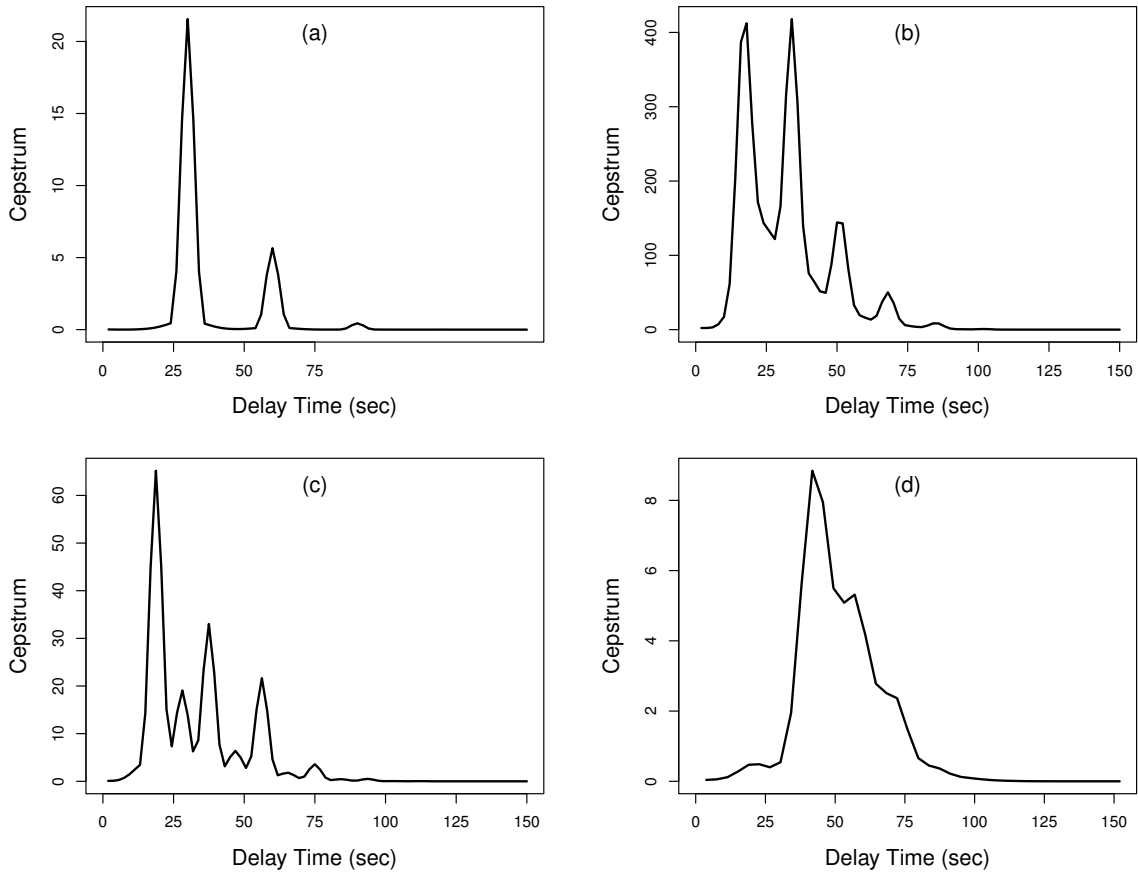


Fig. 9: Cepstra of the detrended spectrum for stimulus times. (a) Constant ripple delay = 30 sec.; (b) Cyclicly repeated ripple delays: 4, 5, 8 sec.; (c) Cyclicly repeated ripple delays: 10, 20, 20, 10 sec.; (d) Stimulus times from the pilot study.

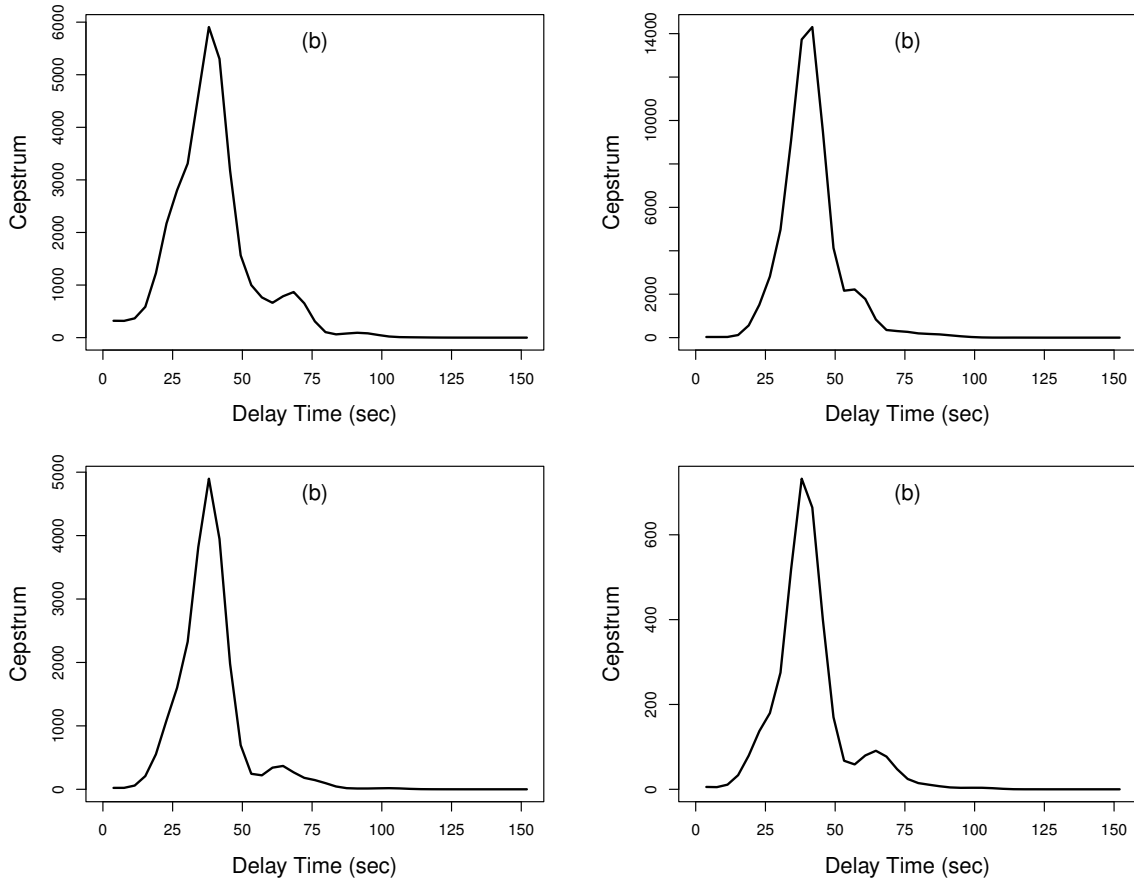


Fig. 10: Cepstra of the detrended spectra for the drift residuals from the 4 voxels shown in Fig.1.